Cao, Ting; Kotnik, Toni; Schwartz, Joseph

Smooth Poly-hypar Surface Structures: Freeform Shells Based on Combinations of Hyperbolic Paraboloids

Published in:
Nexus Network Journal

DOI:
10.1007/s00004-022-00624-w

Published: 01/06/2023

Document Version
Peer-reviewed accepted author manuscript, also known as Final accepted manuscript or Post-print

Please cite the original version:
Cao, T., Kotnik, T., & Schwartz, J. (2023). Smooth Polyhypar Surface Structures: Freeform Shells Based on Combinations of Hyperbolic Paraboloids. *Nexus Network Journal*, *25*(2), 439-463.
https://doi.org/10.1007/s00004-022-00624-w

Smooth poly-hypar surface structures: freeform shells based on combinations of hyperbolic paraboloids

Keyword

Surface structures, freeform shells, descriptive geometry, hyperbolic paraboloids, graphic statics

Abstract

This article presents a new approach to the design of freeform shells--smooth poly-hypar surface structures. As combinations of hyperbolic paraboloids (hypars), smooth poly-hypar surfaces are ruled locally, while globally appearing to be continuous freeform. The double curvature of the individual hypar modules and the smooth connections (G^1 degree) between them ensure global bending-free structural behavior, while the ruled geometrical property of these surfaces allows the relatively lost cost construction. In this article, the structural performance of smooth poly-hypar surface is calculated on two levels with graphic statics: the distribution of internal forces within an individual hypar, and the combination of hypars. It also defines two geometrical constraints of a smooth poly-hypar surface: the coplanarity principle and load paths, which ensure the visual smoothness of the surface and limit only membrane forces transmitted within the global surface. Moreover, several built case studies are presented as applications of smooth poly-hypar surfaces in architectural design, which also show the ease of construction of this new type of double-curved freeform surface.

1. Introduction

1.1 Freeform surface structures

Since the beginning of the 1990s, freeform surfaces have started appearing frequently in architectural design. Such tendency towards form smoothness was derived from the theory of continuity (Lynn, 1993), and interacted with the simultaneous revolution in computer technology, finally aroused a discourse of new architectural forms in digital times (Carpo, 2014) . However, in most cases, freeform surfaces were shallowly treated as a symbol of new digital forms, while the multiple influencing technical factors were ignored. As a result, a series of technical problems in structural performance and construction were raised.

In this case, different approaches in structural and geometrical optimization were explored to improve the structural performance and reduce the construction difficulties of freeform surfaces. From a structural point of view, shells developed from the form-finding method by structural artists (Chilton, 2000) such as Heinz Isler, Sergio Musmeci, and among others were rediscussed in new structuralism to understand the relationship between structural performance and freeform geometry (Oxman & Oxman, 2010). However, these form-finding methods are generally carried out considering given dominant load cases, the resulting freeform shells are only bending-free for a specific load configuration. Moreover, due to their non-developable geometry, there remains quite a lot of difficulties in construction.

Approaches in another direction mainly aimed to reduce energy cost and technical complexity in constructions, by discretizing the freeform surface as a group of developable strips (Flöry, et al., 2013), or approximate freeform surface by *A*-nets, also referred to as hyperbolic nets (Craizer, et al., 2009), (Käferböck & Pottmann, 2013), (Emanuel & Thilo, 2014). These explorations simplified the undevelopable freeform surfaces into the descriptive geometry, thus reduce the complexity of freeform during the construction process. However, the relevant consideration in structural performance is still missing in these researches.

Among these researches, the *A*-net is a special geometry combined from a group of hyperbolic paraboloids(hypars), whose edges intersecting at one node are always coplanar (Emanuel & Thilo, 2014), (Käferböck & Pottmann, 2013). Its basic modules, hyperbolic paraboloids(hypars), due to the high structural performance and construction convention, were applied by several structural engineers and architects of the 20th century in the design of double-curved shells. As shown by the remarkable work of Felix Candela (Mendoza, 2011) (Garlock & Billington, 2008), Eduardo Torroja (Adriaenssens, et al., 2012), Pier Luigi Nervi (Bergdoll, et al., 2010), among others, hypars can be effectively used for the design of complex shell structures. Recently, more researches are developed to explore the discontinuous combinations of hypars in architectural design (Blanco, 2021).

In the existing precedents, hypars are generally combined through folds (Figure 1), which visually lead to interruptions of surface smoothness, and structurally cause stiffening beams to resist bending actions at the folds (Apeland, 1962), (Billington, 1965), (Ramaswamy, 1968), (Mueller, 1977) (Schnobrich, 1971), (Schnobrich, 1988a), (Schnobrich, 1988b), (Domingo, et al., 1999), (Shengzhe Wanga, 2020). However, once the structural advantage of hypars is combined with the geometrical potential of *A*-nets, an innovative approach can be developed to design structurally informed freeform surfaces. Architectural intentions for smoothness, structural requirements for efficiency, and production demands for the economy could all be combined with the help of a new type of freeform surface structures — smooth poly-hypar surface structures (Cao, 2019) (Cao, et al., 2021).

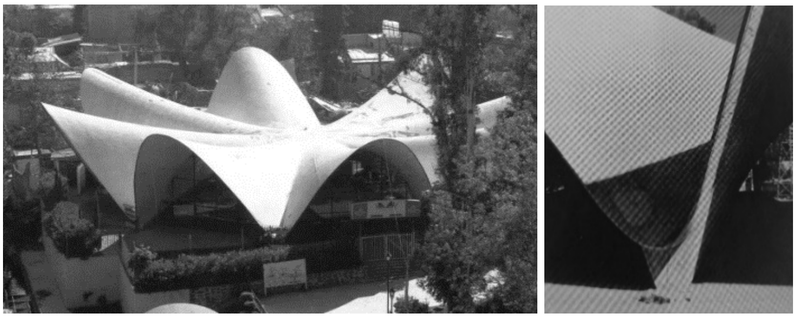

Figure 1: Los Manantiales restaurant designed by Felix Candela. *(Faber, 1963)*. The folded edges of hypar are stiffened with beams.

1.2 Smooth poly-hypar surface structures

From a geometrical point view, smooth poly-hypar surfaces are a special type of A-nets or parabolic nets (Käferböck & Pottmann, 2013). Comparing with A-net, the additional geometrical constraints of a smooth poly-hypar surface results from the requested structural efficiency (section 3.1), called *coplanarity principle*. It differentiates the smooth poly-hypar surface from *A*-nets, which only ensure edges of hypars intersect at one node are coplanar (Cao, 2019).

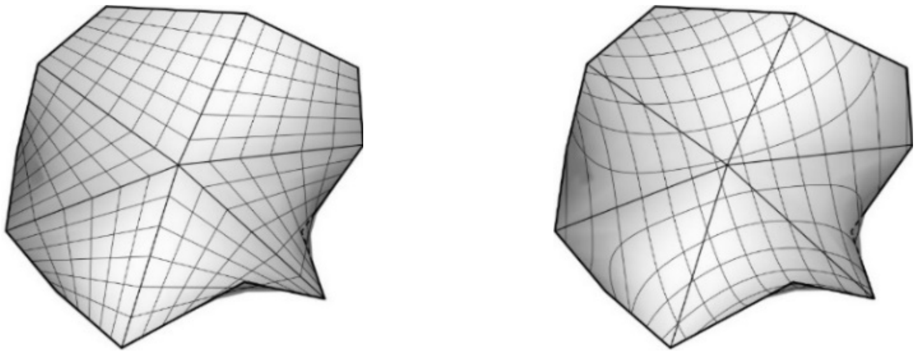

(a) (b)

Figure 2: Smooth poly-hypar surfaces is a special type of A-net. (a) They are locally ruled, (b) while globally are smooth freeform.

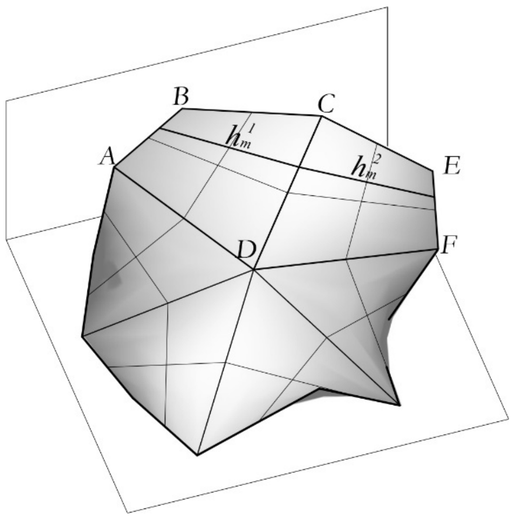

Figure 3 : Following the coplanarity principle, rulings and edges (such as h_m^1, h_m^2 and *BD*)of two adjacent hypars intersecting at one point are always coplanar.

For two adjacent hypars to satisfy the coplanarity principle, the edges of the hypars, represented as vectors, should satisfy the following linear combination (Figure 3 , with *k*, *j, l* scalars and *k*<0), (section 3.1):

$$\overrightarrow{DF} = k\overrightarrow{DA} + j\overrightarrow{DC} \qquad \overrightarrow{CE} = k\overrightarrow{CB} + l\overrightarrow{CD} \tag{1-1}$$

Geometrically, this coplanarity principle ensures the smooth connection between different hypars. Such smoothness satisfies the second-order of continuity - i.e. G^1 continuity and tangency (Mortenson, 2006), (Figure 3a). When $j= l \neq 0$ in (1-1), the smoothness between two adjacent hypars can reach G^2 degree (Figure 3b); when $j= l =0$ in (1-1), it can reach G^3 degree(Figure 3c). While in the case of G^0 degree, two adjacent hypars cannot satisfy the coplanarity principle (that's case in the work of Felix Candela) , there will be bending moment at the shared edges of two adjacent hypars, the geometry is not a smooth poly-hypar surface.

Benefiting from the nature of the individual hypars as ruled surfaces, a smooth poly-hypar surface is globally freeform, but it is locally ruled (Figure 2,Figure 3). This special geometrical property enables the aesthetic expression in architectural design, and also allows the construction convenience.

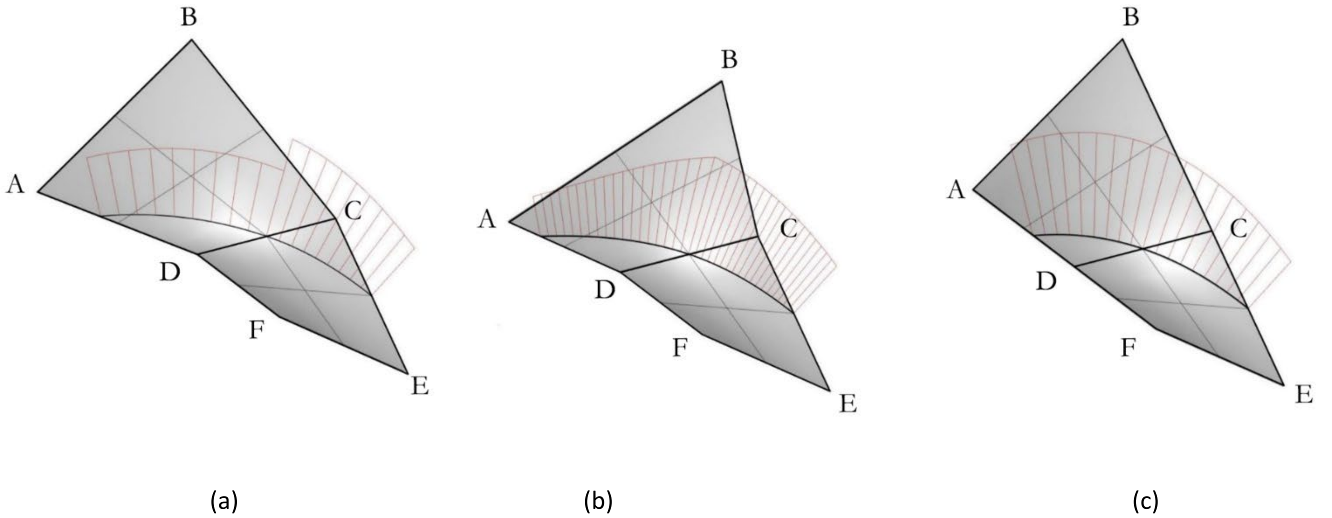

Figure 3: The smoothness between two adjacent hypars in a smooth poly-hypar surface. (a) G^1 degree. (b) G^2 degree. (c) G^3 degree.

1.3 Graphic statics

The structural analysis of single hypar and smooth poly-hypar surfaces developed in the following sections are entirely based on graphic statics. Graphic statics is an equilibrium-based approach that relies on the theory of plasticity (Muttoni, et al., 1997). As a synthetic vector-based structural analysis and design method, it can be described as a set of geometric procedures based on vectors and projective geometry (Maxwell, 1864) (Culmann, 1866) (Cremona, 1890). These geometrical and vectorized properties of graphic statics enable it to become the best mediate to present the relation between forms and forces (Edward & Wacław, 2010), especially in the analysis of hypar geometries, in which the curved surfaces can be represented as groups of vectors (straight rulings), (Figure *4*).

1.4 Content

Generally, the remainder of the article explains in detail the geometrical and structural properties of an individual hypar and its combinations, smooth poly-hypar surfaces. Then, the advantages of this new type of freeform shells in constructions are explained with several built projects.

In section 2, the geometrical definition of a hypar is presented at first. Based on the geometrical and vectorized representation of a hypar, the structural behavior of a hypar is analyzed in detail with graphic statics. Found on the conclusion from section 2, section 3 shows explains two constraints to join hypars into smooth poly-hypar surfaces, which avoid local bending moments meanwhile ensure the global equilibrium of the surface structures. Afterward, a smooth poly-hypar shell is exemplified to calculate its internal forces and reactions in equilibrium. Section 4 presents the application of smooth poly-hypar surfaces in several built prototypes, to show their efficiency in fabrications. Eventually, in the last section, some conclusions are drawn on the main advantages of smooth poly-hypar surfaces in terms of structural performances and fabrication efficiencies. The future potential to optimize the performance of existing freeform geometries with the approximation of smooth poly-hypar surface is also mentioned.

2. Hypar as a module of smooth poly-hypar surfaces

To find out the most efficient way to join hypars into bending-free surfaces (smooth poly-hypar surfaces), this section will study the geometrical properties and structural behavior of an individual hypar with graphic statics at first.

2.1 Geometry of a hypar

This subsection defines in detail the important geometrical objects within a hyperbolic paraboloid (hypar), such as ruling, parabolas, and the axis, which are closely related to the structural performance and construction efficiency of hypar geometries. At the end, the important geometrical terms are defined as formulas of ruling vectors, which are helpful to analyze the structural performance of hypar geometries with graphic statics in the section 2.2 and section3.

A hypar can be constructed geometrically after defining four non-coplanar points *A*, *B*, *C*, and *D* (Figure *4*). Every two consecutive points are connected by an edge of a hypar. The vector from the middle point of diagonal *BD* to the middle point of diagonal *AC* is the axis $\vec{r}$ of the hypar, which passes through the center *O* (Figure *4*). When planes parallel with plane *AOr* and plane *BOr* intersect a hypar, the intersecting curves define two sets of parabolas. The axes of all the parabolas of a hypar are always parallel to the axis

$\vec{r}$(Figure *4*). Axis $\vec{r}$ is a fundamental geometrical parameter of the hypar and it is directly related to its structural behaviour, as it indicates the direction of loads which can be taken by the parabolas of a hypar.

The planes *Ohr* and *Oir* are parallel to edges *AD*, *BC,* and *AB, DC* respectively, (Figure 4b). When a hypar intersects with planes parallel to the plane *Ohr*, one set of straight rulings h_m can be obtained. And another set of rulings i_n are the intersecting lines of the hypar and planes parallel to the plane *Oir*, (m, $n \in Z$), (Figure *4*). To directly relate the geometry of a hypar to its internal forces and reactions, a coordinate system with origin *O* and three coordinate axes *r*, *h,* and *i* (Figure *4*, the dot products $\vec{h} \cdot \overrightarrow{BC} > 0$, $\vec{\imath} \cdot \overrightarrow{AB} > 0$) is set up to represent the hypar surface as two family of ruling vectors: $\vec{h}_m$,$\vec{\imath}_n$ ($m, n \in Z$) , assuming there are *2N* rulings in each family,($N \in Z$).

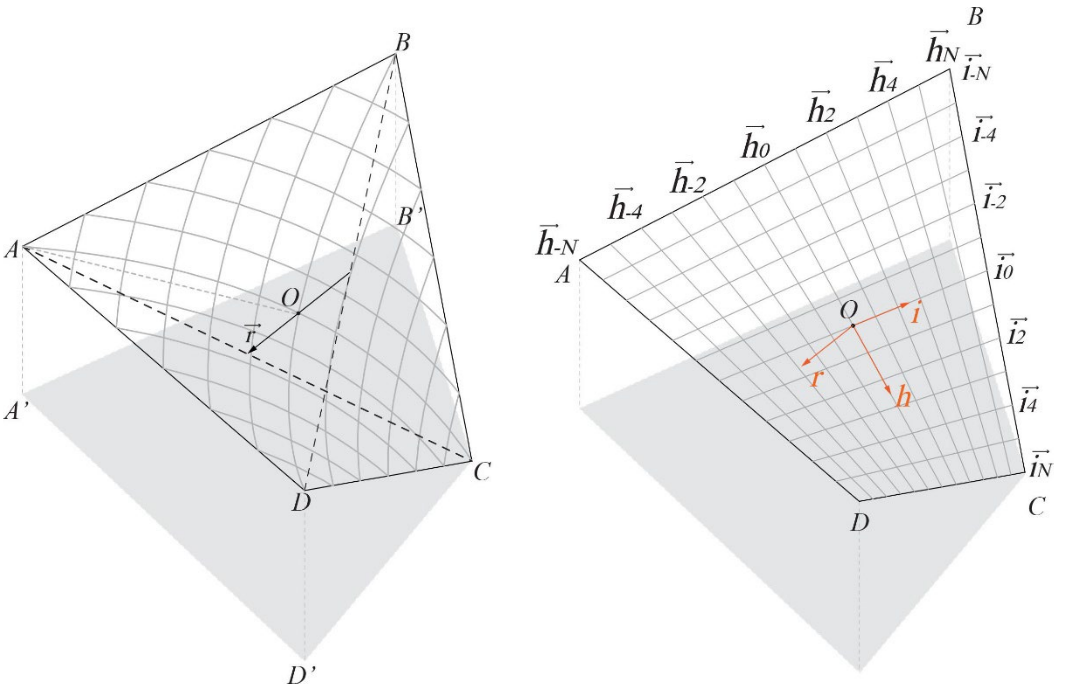

(a) (b)

Figure 4: (a) A hypar defined by four non-coplanar points, there are two sets of parabolas and axis $\vec{r}$ in a hypar. (b)The surface is defined by two sets of vectors in a coordinate system with origin *O* and three coordinate axes *r*, *h,* and *i* .

Axis $\vec{r}$ can always be represented as a linear combination of two vectors in the same family, which can be proven as shown below:

It is trivial that in Figure 4, vector $\vec{r}$ can be written as the sum of vectors $\overrightarrow{AC}$, $\overrightarrow{DA}$ and $\overrightarrow{BD}$:

$$\vec{r} = \frac{1}{2}\overrightarrow{AC} + \overrightarrow{DA} + \frac{1}{2}\overrightarrow{BD} \tag{2-1}$$

By replacing vectors $\overrightarrow{AC}$, $\overrightarrow{BD}$ as sums of vectors $\vec{h}_N$, $\vec{h}_{-N}$, $\vec{\imath}_N$, $\vec{\imath}_{-N}$, (2-1) can be simplified and represented as :

$$\vec{r} = \frac{\vec{h}_N}{2} - \frac{\vec{h}_{-N}}{2} \tag{2-2}$$

Or :

$$\vec{r} = \frac{\vec{\imath}_N}{2} - \frac{\vec{\imath}_{-N}}{2} \tag{2-3}$$

If there are any two rulings $\vec{h}_n$ and $\vec{h}_m$, as it is showed in Figure 5, $\vec{h}_n$ can be always represented as the sum of $\vec{h}_m$, $\vec{\imath}_N$, and $\vec{\imath}_{-N}$:

$$\vec{h}_n = \frac{m-n}{2N}\vec{\imath}_{-N} + \vec{h}_m - \frac{m-n}{2N}\vec{\imath}_N \tag{2-4}$$

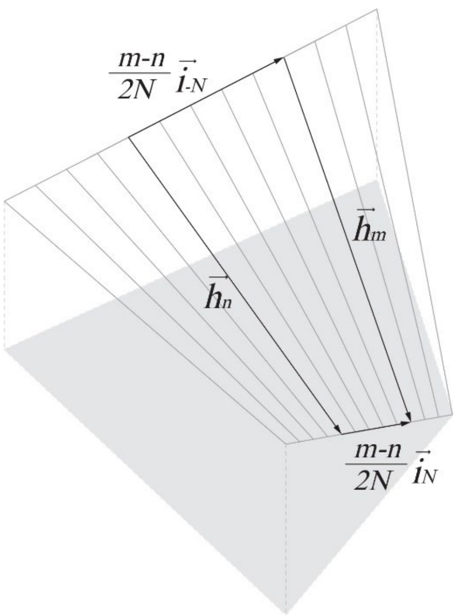

Figure 5:linear relation of rulings $\vec{h}_n$, $\vec{h}_m$, $\vec{\imath}_N$, and $\vec{\imath}_{-N}$.

Rearranging (2-4) and substituting it for $\vec{\imath}_N - \vec{\imath}_{-N}$ in (2-3), gives $\vec{r}$ as a linear combination of $\vec{h}_m$, $\vec{h}_n$:

$$\vec{h}_n - \vec{h}_m = \frac{n-m}{N}\vec{r} \tag{2-5}$$

Similarly, $\vec{r}$ can also be represented as a linear combination of $\vec{\imath}_n$, $\vec{\imath}_m$:

$$\vec{i}_m - \vec{i}_n = \frac{m-n}{N}\vec{r} \tag{2-6}$$

With (2-5) and (2-6), the two important characters of a hypar -- doubly ruled and doubly curved (two sets of rulings and two sets of parabolas) -- are related with each other through formulas of ruling vectors and axis $\vec{r}$. It is helpful to represent all the internal forces and reactions of a hypar by two sets of ruling vectors in the next steps in section 2.2.

2.2 Hypar as a shell in equilibrium

Based on the geometrical properties mentioned above, the internal forces and reactions within a smooth poly-hypar surface can be analyzed and controlled using vector-based graphic statics (D'Acunto, et al., 2019). In this section, a single hypar in an arbitrary position is implemented as a strut and tie model, describing the structural behavior as subsystems in equilibrium. The analysis in this subsection prepares the structural basis to combine single hypars into bending-free surfaces (smooth poly-hypar surfaces) in section 3.

To study the relation between the geometry and the structural behavior of a hypar, a coordinate system (Section 2.1) is introduced to represent all rulings h_m, i_n as ruling vectors $\vec{h}_m$,$\vec{i}_n$ ($m, n \in$ Z), and to number the nodes with coordinates h and i (Figure 6). In the end, all the internal forces and reactions of a hypar can be represented as formulas of ruling vectors $\vec{h}_m$,$\vec{i}_n$.

Compression	
Tension	
Load	
Reaction	
Ruling/Axis component	

Table1: in this paper, the main structural terms are represented in colored graphic.

2.2.1 Redistribution of loads

In a classical hypar with an axis $\vec{r}$ parallel to gravity, all the weight of a hypar are taken by two sets of parabolas *(Candela, 1951) (Apeland, 1962)*. However, when the axis $\vec{r}$ of a hypar is not parallel to gravity, the redistribution of loads in the surface is more complicated.

Assuming there are 2*N* rulings in a hypar ($N \in Z$), the total weight of a hypar is split into N^2 patches. To simplify the calculations, the weight of each patch is considered as the same, then combined as a point load $\vec{g}$ applied at the center of each patch (Figure 6a). A point load applied at any node (*m*,*n*) can be divided into three components (Figure 6b): ruling components $\vec{f}_{h(m,n)}$ and $\vec{f}_{i(m,n)}$ parallel to ruling vectors $\vec{h}_m$ and $\vec{\iota}_n$ respectively, and axis components $\vec{f}_{r(m,n)}$ parallel to axis $\vec{r}$ of the hypar. In this way, it ensures all the loads can be transmitted always in the surface.

Below explains in detail how to calculate these three components $\vec{f}_{h(m,n)}$,$\vec{f}_{i(m,n)}$ and $\vec{f}_{r(m,n)}$ at any node (*m*,*n*).

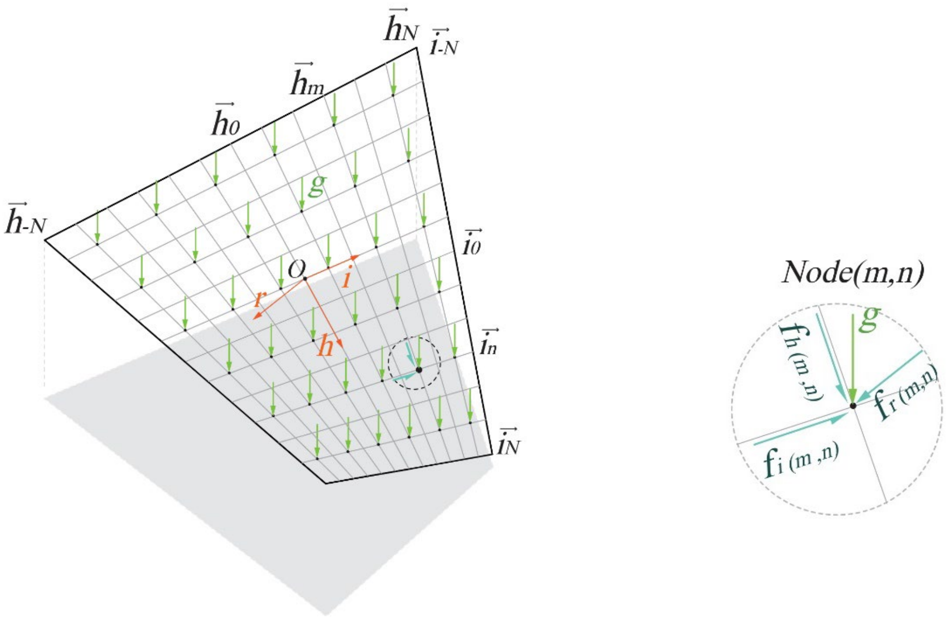

(a) (b)

Figure 6: (a) A hypar is split into N^2 patches, the weight of each patch is combined as a point load $\vec{g}$ applied at the centre of each patch. (b) A point load applied at any node (*m,n*) can be divided into three components: ruling components $\vec{f}_{h(m,n)}$ and $\vec{f}_{i(m,n)}$ parallel to ruling vectors $\vec{h}_m$ and $\vec{\iota}_n$ respectively, and axis components $\vec{f}_{r(m,n)}$ parallel to axis $\vec{r}$ of the hypar.

Assuming a point load $\vec{g}$ at origin *O*, it can be split into three load components concerning the scalars *a*, *b*, *c* of vectors $\vec{h}_0$, $\vec{\iota}_0$ and $\vec{r}$:

$$\vec{g} = a\vec{h}_0 + b\vec{\iota}_0 + c\vec{r} \tag{2-7}$$

Similarly, for a point load $\vec{g}$ at any node (m,n), the three load components can be expressed in relation to the scalars $a_{(m,n)}$, $b_{(m,n)}$, and $c_{(m,n)}$ of vectors $\vec{h}_m$, $\vec{\iota}_n$, and $\vec{r}$:

$$\vec{g} = a_{(m,n)}\vec{h}_m + b_{(m,n)}\vec{\iota}_n + c_{(m,n)}\vec{r} \tag{2-8}$$

According to (2-5) and (2-6), $\vec{h}_m$ and $\vec{\iota}_n$ in (2-8) can be replaced as formulas of $\vec{h}_0$ and $\vec{\iota}_0$, then rewritten as below:

$$\vec{g} = a_{(m,n)}\vec{h}_0 + b_{(m,n)}\vec{\iota}_0 + [c_{(m,n)} + \frac{n}{N}b]\vec{r} \tag{2-9}$$

Comparing (2-8) and (2-9), gotten:

$$a_{(m,n)} = a \quad b_{(m,n)} = b$$

$$c_{(m,n)} = c - \frac{ma+bn}{N} \tag{2-10}$$

From (2-9) and (2-10), a point load $\vec{g}$ at any node (m,n) can be split into ruling components $\vec{f}_{h(m,n)}$, $\vec{f}_{i(m,n)}$ and axis component $\vec{f}_{r(m,n)}$ as below:

$$\vec{f}_{h(m,n)} = a\vec{h}_m \qquad \vec{f}_{i(m,n)} = b\vec{\iota}_n$$

$$\vec{f}_{r(m,n)} = (c - \frac{am+bn}{N})\,\vec{r} \tag{2-11}$$

In this way, the weight of a hypar is redistributed into components parallel to ruling vectors $\vec{h}_m$, $\vec{\iota}_n$ and axis $\vec{r}$ respectively. In the next section, these components will be applied separately onto the hypar, the entire hypar can be regarded as the superposition of two subsystems in equilibrium: subsystem I (Figure 7) and subsystem II (Figure 8).

2.2.2 Construction of Subsystem I in equilibrium

Subsystem I is only loaded with the ruling components $\vec{f}_{h(m,n)}$,$\vec{f}_{i(m,n)}$. To achieve the equilibrium, two edges of the hypar should be supported, and the reactions should have the same magnitude as the internal forces along with rulings but reversed directions (Figure 7).

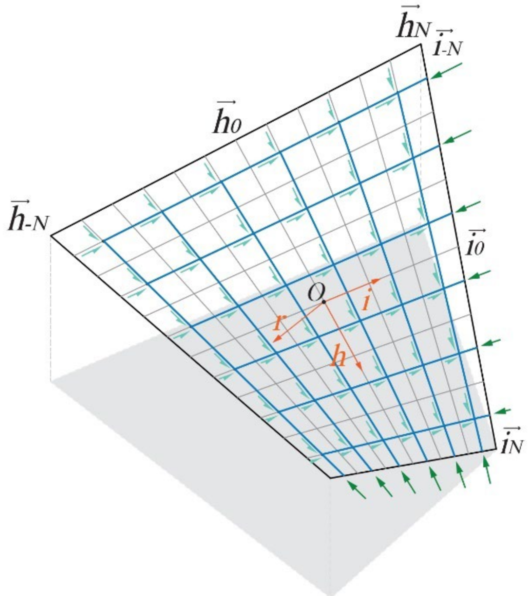

Figure 7:subsystem I is only loaded with ruling components, and internal forces, reactions are parallel to rulings.

Considering that there is *N* number of nodes in the same ruling, according to (2-11), the sum of ruling components along with any ruling h_m and i_n, can be written as follows:

$$\vec{F}_{h(m)\_\mathrm{I}} = Na\vec{h}_m \qquad \vec{F}_{i(n)\_\mathrm{I}} = Nb\vec{\imath}_n \tag{2-12}$$

And the reactions are in the reversed directions and the same magnitude:

$$\vec{R}_{h(m)\_\mathrm{I}} = -Na\vec{h}_m \qquad \vec{R}_{i(n)\_\mathrm{I}} = -Nb\vec{\imath}_n \tag{2-13}$$

2.2.3 Construction of subsystem II in equilibrium

- Redistribution of axis components

Subsystem II is supported at the same edges $\vec{h}_N$, $\vec{\imath}_N$as subsystem I, and only loaded with axis components $\vec{f}_{r(m,n)}$ (Figure 8), which are taken by a group of parabolic cables and a group of parabolic arches in a hypar. To ensure only membrane forces in every parabola, a part of the axis component applied on every parabolic arch, $\vec{f}_{r.arch(m,n)}$ should be the same at every node (*m*,*n*) of the same arch. Similarly, for parabolic cables, the other part of axis component, $\vec{f}_{r.cable(m,n)}$ should also be the same at every node (*m,n*) of the same cable (Figure 8).

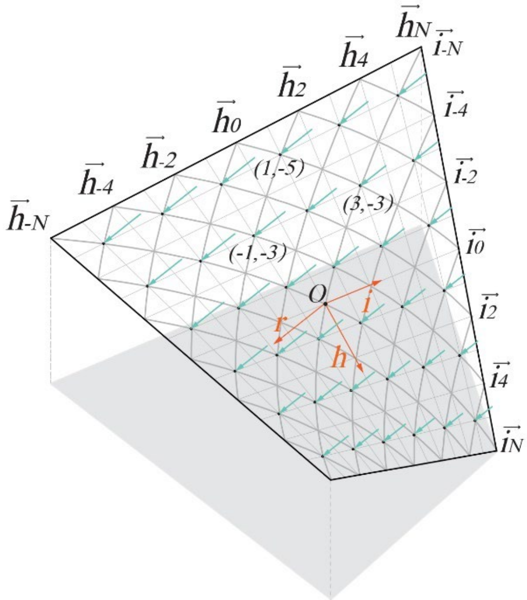

Figure 8:subsystem II loaded with axis components $\vec{f}_{r(m,n)}$.

To achieve the configuration described above, by comparing the value of axis component $\vec{f}_{r(m,n)}$ in (2-11), the part of axis component applied on the cable and arch, respectively$\vec{f}_{r.arch(m,n)}$ and $\vec{f}_{r.cable(m,n)}$, can be written as formulas of $m-n$ or $m+n$, since the difference of two coordinates $m-n$ is the same for every node on the same arch, and $m+n$ is the same for every node on the same cable, (Figure 8):

$$\vec{f}_{r.cable(m,n)} = \left(yc + x\frac{m+n}{N}\right)\vec{r}$$

(2-14)

$$\vec{f}_{r.arch(m,n)} = [(1-y) - \frac{(a+x)m - (-b-x)n}{2N}]\vec{r}$$

(2-15)

where x and y are unknown parameters. To ensure that $\vec{f}_{r.arch(m,n)}$ remains the same when coordinates *m*, *n* vary, it is trivial that in (2-15) the value of $a+x$ should equal to $-b-x$, thus gotten $x = -\frac{a+b}{2}$. To minimize the different between $\vec{f}_{r.arch(m,n)}$ and $\vec{f}_{r.cable(m,n)}$, yc in (2-14) and $(1-y)c$ in (2-15) should be the same, so gotten $y = \frac{1}{2}$. Then (2-14), (2-15) can be rewritten as below:

$$\vec{f}_{r.cable(m,n)} = [\frac{c}{2} - (m+n)\frac{a+b}{2N}]\vec{r}$$

(2-16)

$$\vec{f}_{r.arch(m,n)} = [\frac{c}{2} + (m-n)\frac{b-a}{2N}]\vec{r}$$

(2-17)

(2-16) and (2-17) are the most efficient way to redistribute the axis component $\vec{f}_{r(m,n)}$ applied to cables and arches in a hypar as a continuous shell. However, by varying y, the value and direction of $\vec{f}_{r.arch(m,n)}$ will be different. If the direction of $\vec{f}_{r.arch(m,n)}$ is reversed as the one of axis component $\vec{f}_{r(m,n)}$, the parabolas curving downward will turn from arches into cables, in this case, the whole hypar turns into a prestressed gridshell (Cao, et al., 2021).

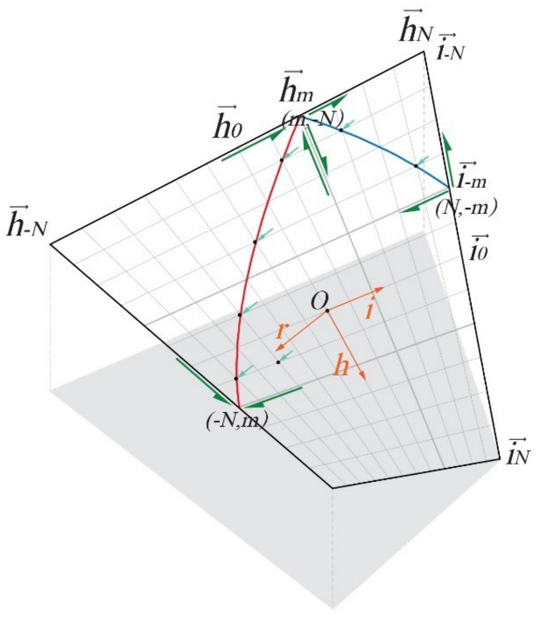

Figure 9: cable *Pl(m,-N / -N,m)* and arch *Pl(m,-N / N, -m)* are loaded with axis components $\vec{f}_{r.arch(m,n)}$ and $\vec{f}_{r.cable(m,n)}$ respectively, supported by rulings and edges.

- Internal forces of parabolas

After setting the $\vec{f}_{r.cable(m,n)}$ in (2-16) for parabolic cables, and $\vec{f}_{r.arch(m,n)}$ in (2-17) for parabolic arches, it is possible to calculate the maximum internal forces and reactions of every parabola in a hypar.

Assuming a parabolic cable $Pl_{(m,-N\,/\,-N,m)}$ in the hypar, with two ends as node (m,-N) and node (-N,m), (Figure 9). According to (2-16), the sum of all the axis components applied on this cable can be written as below:

$$\vec{F}_{r.cable(m,-N/-N,m)} = \left[\frac{c}{2} - (m-N)\frac{a+b}{2N}\right]\frac{N+m}{2}\vec{r}$$

(2-18)

Because the tangents at two ends of cable $Pl_{(m,-N\,/\,-N,m)}$ are coplanar with h_m, i_{-N}, and h_{-N}, i_m respectively, to achieves the equilibrium of cable $Pl_{(m,-N\,/\,-N,m)}$, reactions should be parallel to the rulings h_m, i_m, and edges h_{-N}, i_{-N} (Figure 9). While, according to (2-5) and (2-6), the vectors $\vec{h}_m, \vec{\imath}_{-N}, \vec{h}_{-N}, \vec{\imath}_m$ and $\vec{r}$ are linearly constrained as:

$$\vec{h}_m - \vec{h}_{-N} + \vec{\imath}_m - \vec{\imath}_{-N} = \frac{2(N+m)}{N}\vec{r} \tag{2-19}$$

Comparing (2-18) and (2-19), reactions of cable $Pl_{(m,-N\,/\,-N,m)}$ parallel to the rulings h_m, i_m, and edges h_{-N}, i_{-N} can be written as below:

$$\vec{R}_{h(m)\_cable} = -\left[\frac{c}{2} - (m-N)\frac{a+b}{2N}\right]\frac{N}{4}\vec{h}_m \tag{2-20}$$

$$\vec{R}_{h(-N)\_cable} = \left[\frac{c}{2} - (m-N)\frac{a+b}{2N}\right]\frac{N}{4}\vec{h}_{-N} \tag{2-21}$$

$$\vec{R}_{i(m)\_cable} = -\left[\frac{c}{2} - (m-N)\frac{a+b}{2N}\right]\frac{N}{4}\vec{\imath}_m \tag{2-22}$$

$$\vec{R}_{i(-N)\_cable} = \left[\frac{c}{2} - (m-N)\frac{a+b}{2N}\right]\frac{N}{4}\vec{\imath}_{-N} \tag{2-23}$$

The maximal internal forces at node (m,-N) and node (-N,m), which are two ends of cable $Pl_{(m,-N\,/\,-N,m)}$, should be balanced by the sum of reactions in (2-20) and (2-23), (2-21) and (2-22) respectively, (Figure *10*):

$$\vec{F}_{(-N,m\,)\_cable} = -\left[\frac{c}{2} - (m-N)\frac{a+b}{2N}\right]\frac{N}{4}(\vec{h}_{-N} + \vec{\imath}_m)$$

$$\vec{F}_{(m,-N\,)\_cable} = \left[\frac{c}{2} - (m-N)\frac{a+b}{2N}\right]\frac{N}{4}(\vec{\imath}_{-N} - \vec{h}_m)$$

(2-24)

Similarly, for any parabolic arch $Pl_{(m,-N\,/\,N,\,-m)}$ in the hypar (Figure 9), the reactions parallel to rulings h_m, i_{-m} and edges i_N, h_{-N} can be represented as:

$$\vec{R}_{h(m)\_arch} = \left[\frac{c}{2} + (m+N)\frac{b-a}{2N}\right]\frac{N}{4}\vec{h}_m \tag{2-25}$$

$$\vec{R}_{h(N)\_arch} = -\left[\frac{c}{2} + (m+N)\frac{b-a}{2N}\right]\frac{N}{4}\vec{h}_N \tag{2-26}$$

$$\vec{R}_{i(-m)\_arch} = -\left[\frac{c}{2} + (m+N)\frac{b-a}{2N}\right]\frac{N}{4}\vec{\imath}_{-m} \tag{2-27}$$

$$\vec{R}_{i(-N)\_arch} = \left[\frac{c}{2} + (m+N)\frac{b-a}{2N}\right]\frac{N}{4}\vec{\imath}_{-N} \tag{2-28}$$

By adding (2-25) and (2-28), (2-26) and (2-27) respectively. The maximal internal forces at two ends of arch $Pl_{(m,-N\,/\,N,\,-m)}$ are:

$$\vec{F}_{(m,-N)\_arch} = -\left[\frac{c}{2} + (m+N)\frac{b-a}{2N}\right]\frac{N}{4}(\vec{h}_m + \vec{\imath}_{-N})$$

$$\vec{F}_{(N,-m\,)\_cable} = \left[\frac{c}{2} + (m+N)\frac{b-a}{2N}\right]\frac{N}{4}(\vec{h}_m + \vec{\imath}_{-m})$$

(2-29)

- Reactions parallel to edges

In subsystem II, there are N pieces of cables and arches each intersecting with edge i_{-N} (Figure 9). According to (2-23) and (2-28), reactions accumulated along edge i_{-N} equal to the sum of reactions of all cables and arches intersecting to it :

$$\vec{R}_{i(-N)\_\mathrm{II}} = \sum_{m=-N+2}^{N} \vec{R}_{i(-N)\_cable} + \sum_{m=-N}^{N-2} \vec{R}_{i(-N)\_arch}$$

Which is:

$$\vec{R}_{i(-N)\_\mathrm{II}} = (\frac{c+b}{4}N^2 - \frac{b}{4}N)\,\vec{\iota}_{-N} \tag{2-30}$$

Similarly, reactions parallel to the other three edges i_N , h_{-N} , h_N are respectively (Figure 9):

$$\vec{R}_{i(N)\_\mathrm{II}} = (\frac{b-c}{4}N^2 - \frac{b}{4}N)\,\vec{\iota}_{N} \tag{2-31}$$

$$\vec{R}_{h(-N)\_\mathrm{II}} = (\frac{a+c}{4}N^2 - \frac{a}{4}N)\,\vec{\iota}_{-N} \tag{2-32}$$

$$\vec{R}_{h(N)\_\mathrm{II}} = (\frac{a-c}{4}N^2 - \frac{a}{4}N)\,\vec{\iota}_{-N} \tag{2-33}$$

- Reactions parallel to rulings

In subsystem II, any ruling h_m intersects with four parabolas (Figure *10*): cable $Pl_{(m,-N\,/\,-N,m)}$ and $Pl_{(N,m\,/\,m,N)}$, arch $Pl_{(m,-N\,/\,N,\,-m)}$ and $Pl_{(-N\,,-m/\,m,\,N)}$,which cause four reactions parallel to ruling h_m respectively .

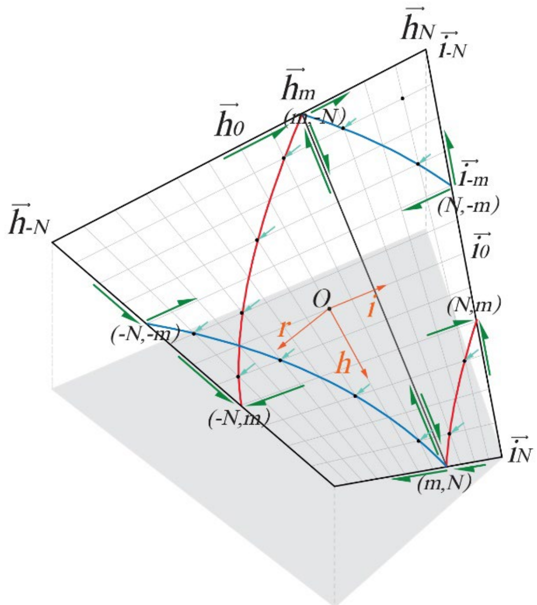

Figure 10: four parabolic arches (blue) and cables(red) are connected with ruling h_m .

The reactions parallel to ruling h_m caused by cable $Pl_{(m,-N\,/\,-N,m)}$ and arch $Pl_{(m,-N\,/\,N,\,-m)}$ are already calculated in (2-20) and (2-25). Following a similar process, it is possible to find reactions caused by cable $Pl_{(N,m\,/\,m,N)}$ and arch $Pl_{(-N,-m/\,m,\,N)}$. By summing up these four reactions, gotten the reactions accumulated along ruling h_m in subsystem II:

$$\vec{R}_{h(m)\_\mathrm{II}} = -\frac{aN}{2}\vec{h}_m \tag{2-34}$$

Similarly, the reactions accumulated parallel to ruling i_n in subsystem II is written as:

$$\vec{R}_{i(n)\_\mathrm{II}} = -\frac{bN}{2}\vec{\imath}_n \tag{2-35}$$

2.2.4 Superposition of two subsystems

By superposing subsystem I and II, it is easy to find that a hypar loaded with self-weight can maintain internal forces as membrane forces, when two edges are fully supported. The maximal internal forces along parabolas can be calculated with formula (2-29), and the necessary reactions are always parallel to rulings and edges as showed in (2-13), and (2-30) to (2-33).

With variations of geometry and position in space, the main behavior of a hypar is changed between a shell and a wall: when axis *r* of a hypar is not parallel to gravity, which is the case in section 2.2, internal forces are along with parabolas, rulings, and edges. The hypar behaves similarly as a combination of a shell and a wall. While, if axis *r* is parallel to gravity, there are only internal forces along with parabolas of a hypar, which behaves like a shell. However, in both cases, the necessary reactions are always parallel to straight rulings and edges of a hypar.

3 Structural behaviour of smooth poly-hypar surface structures

Based on the structural behavior of an individual hypar, it is possible to evaluate the global equilibrium, internal forces and reactions of a smooth poly-hypar surface structure. Only membrane forces are allowed to be transferred within the smooth poly-hypar surface. Such property, on one hand, relies on the structural behavior of an individual hypar, on the other hand, the global stability of a smooth poly-hypar surface which is ensured by the special geometrical constraints, the coplanarity principle (section 1.2) and the fully supported load paths.

This section explains first how the coplanarity principle is achieved to keep the bending-free behavior of a smooth poly-hypar surface, then it analyzes the global equilibrium of a smooth poly-hypar surface structure through the load paths and the special supporting conditions. In the end, the calculations of internal forces, reactions of a smooth poly-hypar surface are presented.

3.1 Local bending-free behaviour and the coplanarity principle

As a combination of hypars, the key point to ensure the structural efficiency of the surface is to avoid bending moment caused by interactions between adjacent hypars. According to the conclusions in section 2.2, interactions, which maintain hypars' internal forces as membrane forces, are always parallel to straight rulings and edges. To ensure these interactions always transmitted in the plane, all the edges and rulings of adjacent hypars intersecting at one node must always be coplanar. When two adjacent hypars satisfy the coplanarity principle (1-1) in section 1.2.

$$\overrightarrow{DF} = k\overrightarrow{DA} + j\overrightarrow{DC} \qquad \overrightarrow{CE} = k\overrightarrow{CB} + l\overrightarrow{CD} \tag{1-1}$$

Which can be proved as below (Figure 11) that any rulings and edges intersect at one node should always be coplanar:

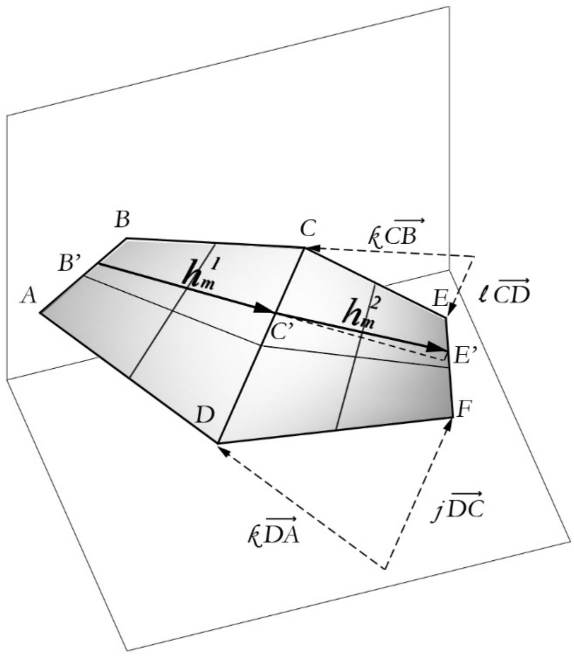

Figure 11: Two adjacent hypars satisfy the coplanarity principle.

$\vec{h}_m^1$ and $\vec{h}_m^2$ (Figure 11) are any ruling vectors on hypar *ABCD* and *CDEF* respectively, intersecting at point C' . Vector $\overrightarrow{B'B}$, $\overrightarrow{C'C}$, $\overrightarrow{E'E}$ can be written as:

$$\overrightarrow{B'B} = x\overrightarrow{AB} \qquad \overrightarrow{C'C} = x\overrightarrow{DC} \qquad \overrightarrow{E'E} = x\overrightarrow{FE} \qquad (0<x<1) \tag{3-2}$$

It is trivial in Figure 11, ruling vector $\vec{h}_m^1$ can be written as the sum of vector $\overrightarrow{B'B}$, $\overrightarrow{BC}$ and $\overrightarrow{C'C}$, by replacing $\overrightarrow{B'B}$ and $\overrightarrow{C'C}$ with $x\overrightarrow{AB}$ and $x\overrightarrow{DC}$ in (3-2) respectively, gotten:

$$\vec{h}_m^1 = x\overrightarrow{AB} + \overrightarrow{BC} - x\overrightarrow{DC} \tag{3-3}$$

In which vector $\overrightarrow{AB}$ can be rewritten as:

$$\overrightarrow{AB} = \overrightarrow{AD} + \overrightarrow{DC} + \overrightarrow{CB} \tag{3-4}$$

Substituting (3-4) for $\overrightarrow{AB}$ in (3-3), gotten:

$$\vec{h}_m^1 = x\overrightarrow{AD} + (1-x)\overrightarrow{BC} \tag{3-5}$$

Similarly, $\vec{h}_m^2$ can be written as:

$$\vec{h}_m^2 = x\overrightarrow{DF} + (1\text{-}\,x)\overrightarrow{CE} \tag{3-6}$$

According to (1-1), (3-6) can be rewritten as:

$$\vec{h}_m^2 = -xk\overrightarrow{AD} - (1-x)k\overrightarrow{BC} + (l - xl - xj)\overrightarrow{DC} \tag{3-7}$$

By comparing (3-5), and (3-7), $\vec{h}_m^2$ can be written as a formula of $\vec{h}_m^1$ and $\overrightarrow{DC}$:

$$\vec{h}_m^2 = -k\vec{h}_m^2 + (l - xl - xj)\overrightarrow{DC} \tag{3-8}$$

Which means rulings vector $\vec{h}_m^1$, $\vec{h}_m^2$ and the shared edge $\overrightarrow{DC}$ are coplanar.

In this case, when two adjacent hypars satisfy the coplanarity principle (1-1), any rulings and edges intersect at one point are always coplanar.

3.2 Global equilibrium and load paths

Benefiting from the coplanarity principle, the interactions of adjacent hypars are always transmitted in the plane without causing bending moment. However,to achieve the global equilibrium, all the interactions should be transmitted to the support finally.

The load path is the way to transmit all the interactions to the supports. Since the internal local forces along parabolas do not affect the global equilibrium, only interactions along rulings and edges are considered in the global equilibrium of smooth poly-hypar surfaces. Considering each hypar as a sub-system in equilibrium, the reactions at the border of one hypar are transferred as actions into the adjacent hypars. In this case, hypars in a smooth poly-hypar surface are supported one by another until all the forces are transmitted to the supports (Cao & Schwartz, 2017), (Figure 13). Based on the coplanarity principle, all intersecting rulings and edges of two adjacent hypars are always coplanar. This geometric property implies that the interaction forces between adjacent hypars are always transmitted along with rulings and edges, thus generating specific load paths (Figure 12) to transfer the internal forces to the supports (Cao & Schwartz, 2017).

In this way, the designer can combine hypars freely as long as the coplanarity principle is fulfilled and each load path is directly connected to a support.

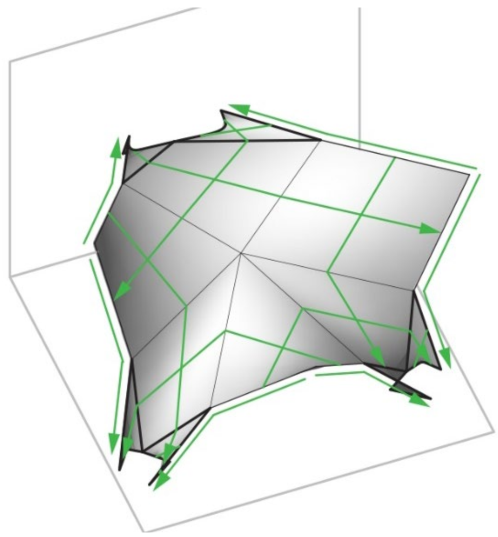

Figure 12: load paths parallel to middle rulings in a smooth poly-hypar surface supported by the ground and the side wall.

3.3 Internal forces and reactions of smooth poly-hypar surface structures

In a smooth poly-hypar surface, the reactions of a hypar are transferred as action forces applied at the border of an adjacent hypar. As the hypar analyzed in section 2.2, the reactions $\vec{R}_h$ and $\vec{R}_i$ along any rulings and edges can be reversed as input action forces $\vec{F}_h$ and $\vec{F}_i$ in the global equilibrium of a smooth poly-hypar surface structure (Cao & Schwartz, 2017). Action forces $\vec{F}_h$ and $\vec{F}_i$ along rulings and edges of one hypar should be the same magnitude but opposite to the directions of reactions $\vec{R}_h$, $\vec{R}_i$.

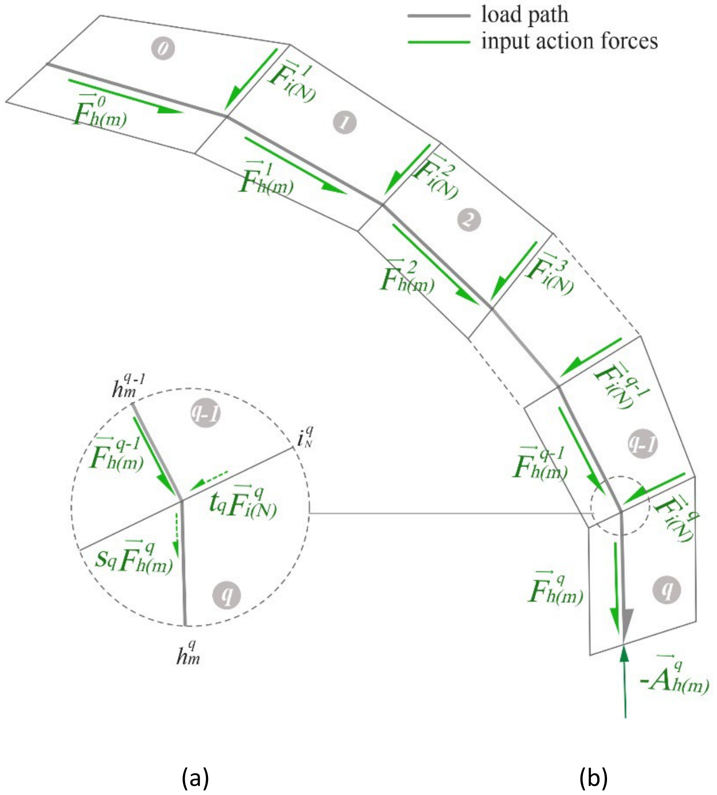

Figure 13: A group of hypars in a smooth poly-hypar surface supported one by another, forming load paths to transmit loads to the group. (b) A special load path is showed as an example. (a) The action force $\vec{F}_{h(m)}^{(q-1)}$ along ruling $h_m{}^{q-1}$ can be decomposed into two components parallel to ruling $h_m{}^q$ of and edge $i_N{}^q$.

These action forces are accumulated and transmitted along load paths formed by rulings and edges, causing internal forces and reactions of a smooth poly-hypar surface. Below it studies particularly the internal forces along with rulings h_m (m∈ Z) of this group of hypars. The position of hypar along the load path is numbered as *q* from zero (Figure *13*).

According to the coplanarity principle and load paths, the action force $\vec{F}_{h(m)}^{(q-1)}$ along ruling $h_m{}^q$ can be decomposed into two components parallel to ruling $h_m{}^q$ and edge $i_N{}^q$ (Figure 13).

$$\vec{F}_{h(m)}^{(q-1)} = s_q \vec{F}_{h(m)}^{q} + t_q \vec{F}_{i(N)}^{q} \tag{3-9}$$

where s_q , t_q are vector scalars of the action force $\vec{F}_{h(m)}^{q}$ and $\vec{F}_{i(N)}^{q}$ respectively; *m* represents the number of rulings *h*; *i(N)* represent one edge of a hypar *q* represents the position of the hypar along the load path.

As it shows in Figure 13, all the hypars that precede hypar H_q along the same load path generate components that are eventually accumulated at the ruling $h_m{}^q$ of hypar H_q. According to (3-7), internal forces accumulated along any ruling $h_m{}^q$ can be written as the sum of *q+1* parts components in (3-8), (Cao, et al., 2021):

$$\vec{A}_{h(m)}^{q} = \left(1 + \sum_{j=1}^{q} \prod_{l=j}^{q} s_l\right) \vec{F}_{h(m)}^{q} \tag{3-10}$$

where s_l are vector scalars of the action force $\vec{F}_{h(m)}^{q}$; in the index of the action force $\vec{F}_{h(m)}^{q}$, m represents the number of rulings; q represents the position of the hypar along the load path.

By decomposing the accumulated force $\vec{A}_{h(m)}^{q-1}$ along ruling h_m^{q-1} into two components along ruling h_m^{q} and edge i_N^{q}, (Figure 13) we can get the deviation force accumulated along edge i_N of hypar H_q as (Cao, et al., 2021):

$$\vec{D}_{i(N)}^{q} = t_q \left(1 + \sum_{j=1}^{q-1} \prod_{l=j}^{q-1} s_l\right) \vec{F}_{i(N)}^{q} \tag{3-11}$$

The deviation force $D_{i(N)}^{q}$ along the edge i_N^{q} in Figure 13 can be added with the action force $\vec{F}_{i(N)}^{q}$, and treated again as an input action force parallel to rulings and transmitted into the supports through other load paths. Using Equations (3-8) and (3-9) repeatedly, the final accumulated internal forces along rulings and edges can be calculated until the deviation forces along the edges are all connected with the supports directly.

From (3-8) and (3-9), we can find that reactions along with rulings and edges of a smooth poly-hypars surface, which are the same magnitude but different directions of (3-8) and (3-9), only depends on the action force $\vec{F}_h$ and $\vec{F}_i$. If the total loads and geometry are the same, the resulted actions $\vec{F}_h$ and $\vec{F}_i$ always keep the same when the hypars are implemented either as continuous shell or prestressed gridshell (Cao, et al., 2021). That means, no matter a smooth poly-hypar surface is built as a rigid continuous shell or a prestressed gridshell, if the total load applied on the surface structure is the same, the reactions to keep the global equilibrium always remain unchanged.

4 Construction Prototypes

Smooth poly-hypar surfaces have been applied in the design and construction of several shell structures. Their special geometrical properties enable not only structural efficiency but also construction convenience for double-curved surface structures.

Since the structural analysis based on graphic statics is materially independent, smooth poly-hypar surfaces can be implemented as different material systems, either as rigid shells or prestressed gridshells. As rigid shells, smooth poly-hypar surfaces were built with material that can take both compressions and tensions, such as plywood in the fabrication of Hypar Wave, a shelter for a temporary open theatre (Figure 14); or ferrocement used to construct Hypar Cantilever (Figure 16). While, as a prestressed gridshell, parabolas in each hypar module can be built as cables in tension, while straight elements as aluminium rods, like the case of Hypar Pavilion, a temporary campus installation (Figure 15).

Generally speaking, there are several advantages of smooth poly-hypar surface in terms of construction:

(a)

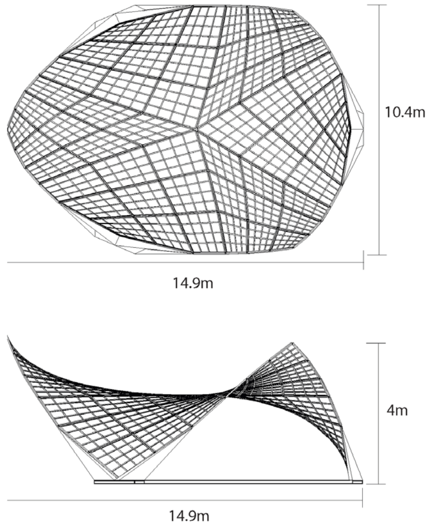

(b)

Figure 14: (a) a shelter for a temporary open theatre, Hypar Wave, was built with prefabricated plywood modules and assembled in site . (b) Elevation and plan of Hypar Wave.

- <u>Low-tech and low-cost prefabrications</u>: Benefiting from the ruled geometry, smooth poly-hypar surfaces can be prefabricated in modules separately using straight elements instead of customized curved components, which effectively reduce the construction cost and complexity. In Hypar Pavilion, a prestressed grid shell (Figure 15), the hypar modules of the shell were prefabricated with straight aluminium rods manually; and in the case of Hypar Wave, a timber grid shell (Figure 14), each hypar module was made with timber strips twisted manually with a tool; or in the test of a ferrocement shell, straight reinforcement bars were welded into a metal grid (Figure 16), covered with steel mesh, then working as a lost formwork for concrete casting.
- <u>Minimized scaffoldings</u>: Due to the local stiffness of double-curved geometries, lightweight hypar modules can be assembled starting from the ground up to the top of the structure without the

complex scaffolding require (Cao, et al., 2021). As the combination hypar modules can be self-supported during the whole dynamic assembly process, only some temporary supports are necessary.

- <u>Reusable components</u>: Benefiting from the straight elements of hypar modules and mechanical joints, all the elements can be dissembled and reused in another design layout. Such as the case of a prestressed grid shell—Hypar Pavillion (Figure 15), up to 80 percent of rods were cut into standard lengths, and connected through standardized joints (Cao, et al., 2021). it was first built at the campus of the Southeast University of Nanjing , then disassembled and subsequently moved around 700 kilometres away to the city of Dezhou, to be reassembled for a second exhibition. This proved the success of the proposed temporary and reusable fabrication concept.

(a)

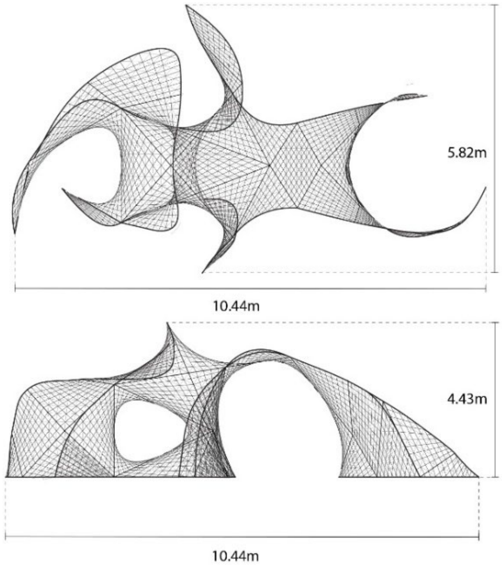

(b)

Figure 15: (a) Hypar Pavillion as a prestressed gridshell made from alumini rods and steel cablse.(b) Plan and elevation of Hypar Pavillion, which is combined from 64 pieces of hypars

Figure 16: A test of ferrocement shell in the construction of hypar cantilever.

5 Conclusion

Smooth poly-hypar surfaces, a modular system of hypars, achieve the smoothness called for in the design of freeform architecture, while simultaneously including technical consideration in structural performance and fabrication efficiency. As the structural analysis presented in this article, the coplanarity principle and load path enable smooth poly-hypar surfaces under distributed loads free of bending moment, meanwhile keep the visual smoothness of the surface. While the locally ruled properties of smooth poly-hypar surfaces also enable simple and economic methods to fabricate complex double-curved surfaces.

This innovative surface geometries could also enable a structural and geometrical optimization of existing complex freeform surfaces. In the current research of freeform optimization, the complex freeform surfaces are normally approximated with planar surfaces or ruled strips (Flöry, et al., 2013), which cannot lead to smooth approximations of the original geometries, neither improvement of structural behaviour. When using smooth poly-hypar surfaces though, the resulting approximations are always smooth. Although the difference between the original surfaces and the approximation still exists. If this difference doesn't affect the architectural expression of the original geometry, the approximated geometry generated following the principle of smooth poly-hypar surfaces certainly leads to more advantages in structural efficiency and construction convenience.

References

Adriaenssens, S., Brown, N., Lowinger, R. & Hernandez, J., 2012. Structural Analysis of Reinforced Concrete Folded Hyperbolic Paraboloid: A Case Study of the Modern Miami Marine Stadium. *International Journal of Architectural Heritage,* 8(4), pp. 498-516.

Apeland, K., 1962. *On the Analysis the Bending Stress in Shallow Hyperbolic Paraboloidal Shells.* San Francisco, World Conference on Shell Structures.

Bergdoll, B. et al., 2010. *Pier Luigi Nervi: Architecture as Challenge.* Milan: Silvana Editoriale.

Billington, D. P., 1965. *Thin Shell Concrete Structures.* New York: McGRAW-HILL Book.

Blanco, F. L. d., 2021. Virtual reconstruc□ on and geometric analysis of Félix Candela's. *DISEGNARECON,* 14(27).

Candela, F., 1951. Structural Application of Hyperbolic Paraboloidical Shell. *Journal of the American Concrete Institute,* 51(20), pp. 397-415.

Cao, T., 2019. *Smooth Poly-Hypar Surface Structures,* Zurich: ETH Zurich.

Cao, T. et al., 2021. Design of Prestressed Gridshells as Smooth Poly-hypar Surface Structures. *Structures,* p. 973–984.

Cao, T. & Schwartz, J., 2017. *The Global Equilibrium of Hypar-combined Shells Based on the Method of Graphic Statics.* Hamburg, IASS Conference 2017.

Carpo, M., 2014. Ten Years of Folding. In: R. Oxman & R. Oxman, eds. *Theories of the Digital in Architecture.* London: Routledge, pp. 38,39, 41.

Chilton, J., 2000. *The Engineer's Contribution to Contemporary Architecture, Heinz Isler..* London: Thomas Telford.

Craizer, M., Anciaux, H. & Lewiner, T., 2009. Discrete Affine Minimal Surfaces with Indefinite Metric. *Differential Geometry and its Applications,* 28(2), pp. 158-169.

Cremona, L., 1890. *Polygon of Forces and Funicular Polygon as Reciprocal Figures in Graphic Statics.* Oxford: Oxford University Press.

Culmann, K., 1866. *Die graphische Statik.* s.l.: Meyer und Zeller.

D'Acunto, P. et al., 2019. Vector- based 3D Graphic Statics: A Framework for the Design of Spatial Structures Based on the Relation between Form and Forces. *International Journal of Solids and Structures,* Volume 167, pp. 58-70.

Domingo, A., Lázaro, C. & Serna, P., 1999. *Design of a Thin Shell Steel Fiber Reinforced Concrete Hypar Roof.* Madrid, IASS Symposium 1999.

Edward, A. & Wacław, Z., 2010. *Form and Forces : Designing Efficient, Expressive Structures.* Hoboken: Wiley.

Emanuel, H.-V. & Thilo, R., 2014. Discretization of Asymptotic Line Parametrizations Using Hyperboloid Surface Patches. *Geometriae Dedicata,* 168(1), pp. 265-289.

Faber, C., 1963. *Candela / The Shell Builder.* New York: Reinhold Publishing Corporation.

Flöry, S. et al., 2013. *Ruled Free Forms.* Vienna, Springer.

Garlock, M. E. M. & Billington, D. P., 2008. *Félix Candela : Engineer, Builder, Structural Artist.* Princeton: Princeton University Art Museum.

Käferböck, F. & Pottmann, H., 2013. Smooth Surfaces from Bilinear Patches: Discrete Affine Minimal Surfaces. *Computer Aided Geometric Design,* 30(5), pp. 476-489.

Lynn, G., 1993. Architectural Curvilinearity: the Folded, the Pliant and the Supple. *Architectural Design,* 63(1-4), p. 25.

Maxwell, J., 1864. On Reciprocal Figures, Frames and Diagrams of Forces. *Philosophical Magazine,* 250(61), p. 27.

Mendoza, M. R., 2011. Félix Candela's Legacy: An Investigation of Félix Candela's Work and its Legacy to the Sociocultural Heritage and Public Identity of the Contemporary Society in Mexico and the UK. In: J. NUNES, ed. *RIBA Education Yearbook 2011.* London: Royal Institute of British Architects, pp. 126-131.

Mortenson, M. E., 2006. *Geometric Modeling.* New York: Industrial Press.

Mueller, G., 1977. *Nonlinear Analysis of Reinforced Concrete Hyperbolic Paraboloid Shells,* Berkeley: Department of Civil Engineering,University of California.

Muttoni, A., Schwartz, J. & Thürlimann, B., 1997. *Design of Concrete Structures with Stress Fields.* Basel: Birkhäuser.

Oxman, R. & Oxman, R., 2010. The New Structuralism: Design, Engineering and Architectural Technologies. *Architectrual Design,* 80(4), pp. 14-23.

Ramaswamy, G. S., 1968. *Design and Construction of Concrete Shell Roofs.* New York: McGraw-Hill.

Schnobrich, W., 1971. Analysis of Hyperbolic Paraboloid Shells. *Concrete Thin Shells,* ACI Special Publication(P-28), pp. 275-312.

Schnobrich, W., 1988a. Hyperbolic Paraboloid Shell Structures. In: J. Christiansen, ed. *Hyperbolic Paraboloid Shells: State of the Art.* Detroit: American Concrete Institute, pp. 1-15.

Schnobrich, W., 1988b. Bending Theory. In: J. Christiansen, ed. *Hyperbolic Paraboloid Shells: State of the Art.* Michigan: American Concrete Institute, p. 5.

Shengzhe Wanga, A. L. M. G. J. A. C.-J., 2020. Structural evaluation of Félix Candela's 8-sided hyperbolic paraboloidal. *Engineering Structures,* Volume 222, pp. 1-14.